Surficial Deposits at Gusev Crater Along Spirit Rover Traverses

J. A. Grant,[1]* R. Arvidson,[2] J. F. Bell III,[3] N. A. Cabrol,[4] M. H. Carr,[5] P. Christensen,[6] L. Crumpler,[7] D. J. Des Marais,[8] B. L. Ehlmann,[2] J. Farmer,[6] M. Golombek,[9] F. D. Grant,[6] R. Greeley,[6] K. Herkenhoff,[10] R. Li,[11] H. Y. McSween,[12] D. W. Ming,[13] J. Moersch,[12] J. W. Rice Jr.,[6] S. Ruff,[6] L. Richter,[14] S. Squyres,[3] R. Sullivan,[3] C. Weitz[15]

The Mars Exploration Rover Spirit has traversed a fairly flat, rock-strewn terrain whose surface is shaped primarily by impact events, although some of the landscape has been altered by eolian processes. Impacts ejected basaltic rocks that probably were part of locally formed lava flows from at least 10 meters depth. Some rocks have been textured and/or partially buried by windblown sediments less than 2 millimeters in diameter that concentrate within shallow, partially filled, circular impact depressions referred to as hollows. The terrain traversed during the 90-sol (martian solar day) nominal mission shows no evidence for an ancient lake in Gusev crater.

Gusev crater is 160 km in diameter, is of Noachian age, and lies at the terminus of the 900-km-long branching Ma'adim Vallis. The crater is partially filled by Hesperian-aged materials (*1*) and was selected as the landing site for the Mars Exploration Rover Spirit to search for evidence of previous liquid water flow and/or ponding that may be responsible for the crater infilling (*1*–*8*).

Landing occurred on a generally flat plain (14.5692°S, 175.4729°E) characterized by approximately circular, shallow depressions <20 m in diameter [hollows (*9*)] (Fig. 1A) and poorly defined ridges up to hundreds of meters long and a few meters high (Plate 1). The 210-m diameter Bonneville crater (*9*) is ~300 m northeast of the lander, and surface albedo increases from ~0.19 to ~0.26 toward its rim as a result of increased dust mantling (*10*). Bonneville and its ejecta deposits comprised the primary exploration targets along the 506-m traverse during the nominal mission reported here.

The largest rocks within 20 m of the lander are <0.5 m in diameter, smaller than the largest rocks at the three previous Mars landing sites (*11*, *12*). Rocks >1 cm cover about 5% of the surface, and the area covered by fragments >10 cm is ~50% of the total rock-covered area (*12*). The size-frequency distribution of rocks >1 cm generally follows the exponential model distribution based on the Viking Lander and Mars Pathfinder landing sites for 5% rock abundance (*1*, *11*).

Most rocks >1 cm are angular to subangular (*13*) and of variable sphericity (*13*), and almost none display obvious rounding (*14*). The majority of rocks are intrinsically dark gray in color, but some exhibit variable dust coverings and possibly associated weathering coatings or rinds that impart a light-toned and/or reddish color, especially apparent on the lowermost 5 to 15 cm of their surfaces (*10*–*12*, *15*, *16*) (Plate 9). Bulk-rock compositions are consistent with picritic (olivine-rich) basalt (*16*).

Rocks >15 cm and within 20 m of the lander are mostly around hollows or near drift deposits, whereas they are largely absent within hollows (Fig. 1A). Rocks sitting exposed or perched on the surface are up to 10 times as numerous around the immediate exterior of hollows as elsewhere (Fig. 1A). Fractured and split rocks are also concentrated around the hollows, but lighter toned (redder) rocks are often closer to eolian drifts. Faceted rocks are five to eight times as abundant away from hollows (Fig. 1B) and are likely the result of wind erosion (*15*).

There are six times as many rock fragments <4 cm in diameter per m^2 as at the Pathfinder landing site and 36 times as many per m^2 as at either of the Viking Landers (*17*). Rocks <2 mm comprise regolith and local drift deposits covering much of the surface. These fine sediments are characterized by bimodal size distributions having modes between 1 and 2 mm in diameter and less than about 0.5 mm in diameter (*18*). The coarser 1- to 2-mm grains are often rounded (*14*), perhaps the result of abrasion during transport. Grains <0.2 mm in diameter comprise about 30% of the samples, are typically basaltic in composition and devoid of clays and aqueous weathering products (*16*), but are too small to be characterized more completely (*18*).

The largest rocks within 10 m of the traverse to Bonneville's rim increased by a factor of five to at least 2.5 m in diameter across the crater's outer discontinuous ejecta (where the deposit incompletely buries the preimpact surface) and more proximal continuous ejecta (where the deposit completely buries the preimpact surface), which starts about 205 m and 175 m from the rim, respectively (Fig. 2). Partial burial of some of the largest rocks along Bonneville's rim precludes accurate measure of their maximum diameter, but those that are visible confirm an exponential increase in number with decreasing size. By contrast, the average size of rocks <10 to 15 cm increases by a factor of less than two, from 1.75 to 2.95 cm, along the traverse while their relative sorting decreases (Table 1).

The rim of Bonneville crater (Plates 3 and 5) rises 6.4 m above the surrounding plain, and the crater averages 10 m deep, with a maximum floor-to-rim-crest relief of 14 m. Wall slopes measured along 32 evenly spaced lines by using two different stereo panoramas average 11°, with a range between 6° and 16°. Although a cover of eolian drift mantles the crater floor and portions of the walls (*10*, *15*), rocks poking up through the drift in a few locations suggest that most of the deposits are relatively thin (less than a meter or two thick). Crater walls are locally steepest and convex along the southeast wall, where some of the largest boulders protrude and where several small craters (12 to 15 m in diameter) excavated the eastern wall.

Several lines of evidence suggest that Bonneville was formed into unconsolidated

[1]Center for Earth and Planetary Studies, National Air and Space Museum, Smithsonian Institution, Washington, DC 20560, USA. [2]Department of Earth and Planetary Sciences, Washington University, St. Louis, MO 63130, USA. [3]Department of Astronomy, Space Sciences Building, Cornell University, Ithaca, NY 14853, USA. [4]NASA Ames/SETI Institute, Space Science Division, MS 245-3, Moffett Field, CA 94035, USA. [5]U.S. Geological Survey, 345 Middlefield Road, Menlo Park, CA 94025, USA. [6]Department of Geological Sciences, Arizona State University, Tempe, AZ 85287, USA. [7]New Mexico Museum of Natural History and Science, 1801 Mountain Road NW, Albuquerque, NM 87104, USA. [8]NASA Ames Research Center, Moffett Field, CA 94035, USA. [9]Jet Propulsion Laboratory, California Institute of Technology, Pasadena, CA 91109, USA. [10]U.S. Geological Survey, Flagstaff, AZ 86001, USA. [11]Department of Civil and Environmental Engineering and Geodetic Science, Ohio State University, Columbus, OH 43210, USA. [12]Department of Earth and Planetary Sciences, University of Tennessee, Knoxville, TN 37996, USA. [13]NASA Johnson Space Center, Houston, TX 77058, USA. [14]DLR Institute of Space Simulation, Linder Hoehe, D-51170, Cologne, Germany. [15]NASA Headquarters, 300 E Street S.W., Washington, DC 20560, USA.

*To whom correspondence should be addressed. E-mail: grantj@nasm.si.edu

Table 1. Small rock size and sorting. Rocks <10 to 15 cm per m^2, sorting based on comparison of measured variance.

Location*	Average long axis (cm)	Variance (cm)
Spirit landing site	1.75	0.99
Bonneville discontinuous ejecta	1.96	1.68
Bonneville continuous ejecta	2.95	1.91

*Measured in 1 m^2 grids with standardized Pancam and end-of-drive clast surveys.

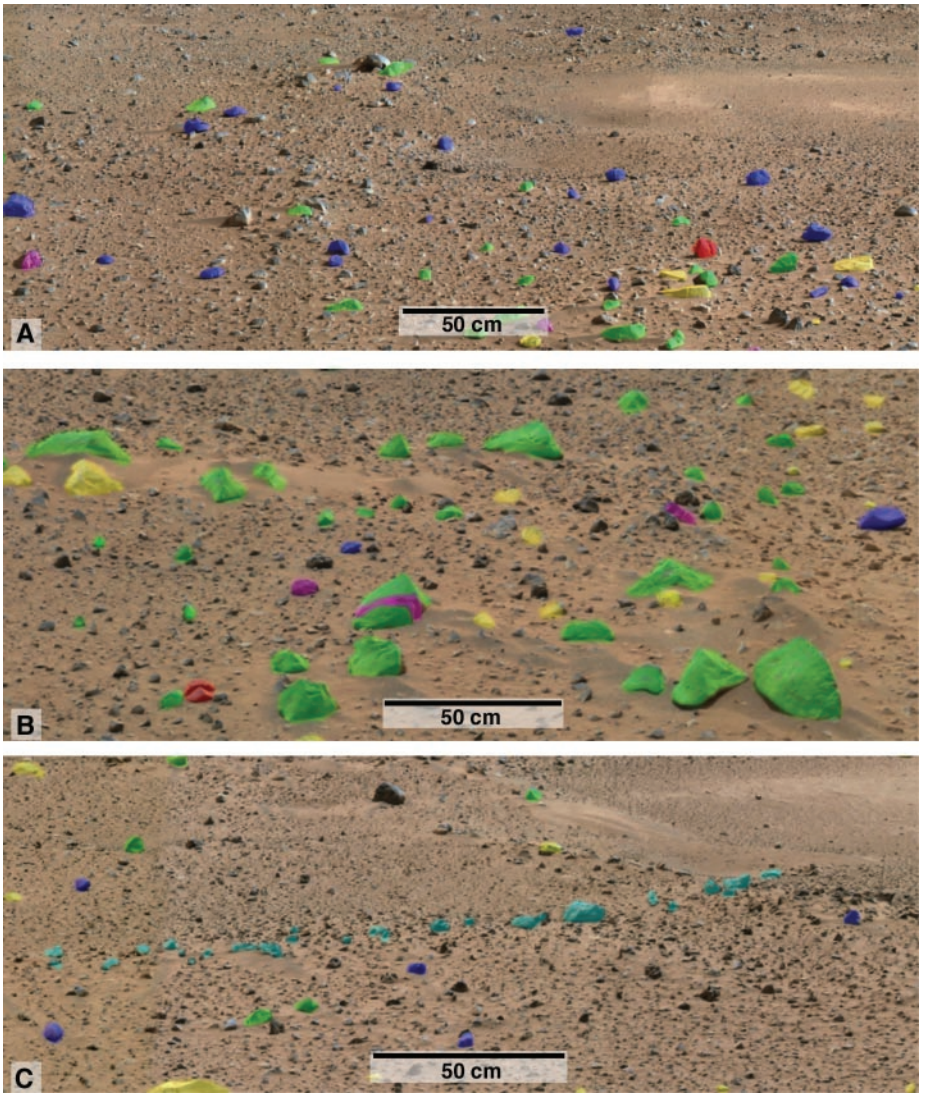

Fig. 1. Example rock types around the lander. (**A**) Perched (blue), split (red), and fractured (purple-pink) rocks are 2 to 10 times as numerous around hollows as elsewhere (azimuth shown is 160° to 195°). (**B**) Faceted (green) and light-toned (yellow) rocks are concentrated around drift, with faceted rocks five to eight times as numerous (azimuth shown is 70° to 95°). (**C**) Radial accumulation of blocks (light blue) around hollow (azimuth shown is 260° to 285°). Mapped on Pancam Mission Success panorama (mspan_2X_final-A1OR1_br, approximate true color based on a scaling of 750-nm, 530-nm, and 480-nm filter data as RGB) (see Plate 1) and emphasized blocks >10 cm in diameter up to 20 m from the lander. Near-field scales are approximate.

blocky debris. First, the low wall slopes indicate that coherent strata did not impede slumping during final stages of crater formation. Second, the largest rocks appear jumbled and reflect local transport after disruption of rocks up to 6 m in diameter during the late stages of crater formation (*19*). Third, the small craters formed into the eastern wall of Bonneville do not expose bedrock. Finally, the sharp contrast between Bonneville's ejecta deposits (Fig. 2) and surfaces beyond the ejecta (e.g., surrounding the lander) indicate that surfaces of the crater facies remain relatively pristine and are not mantled by younger debris that might mask detection of bedrock in the crater walls. We conclude that the crater formed largely in loose rubble but that the largest observed ejecta blocks may be derived from locally more competent rocks (e.g., a lava flow).

Despite shallow wall slopes relative to many pristine primary craters (*20*), the absence of debris chutes and subjacent talus at their base and uniformly distributed rocks on the walls imply that there has been little modification of the walls by mass wasting. In addition, relatively drift-free sections of the walls (Plates 3 and 5) retain low slopes, which demonstrates that eolian infilling is not responsible for masking steeper walls. Instead, the well-preserved character and low depth-to-diameter ratio of ~0.07 suggests that Bonneville crater experienced meters or less of erosion and may have formed during a secondary cratering event (*21*).

Hollow morphology and sizes (Fig. 3) argue for an impact origin. Their spatial distribution across most surfaces is random [figure 1A in (*22*)] and characterized by a population that increases exponentially from 20 m down to less than 1 m (Fig. 3), consistent with that expected for small craters (*23*–*25*). Hollows have fairly uniform morphology, and the increased perched, fractured, split, and sometimes radial distribution of rocks around their margins (Fig. 1C) is consistent with emplacement as ejecta. Although the number density of hollows decreases within about 100 m of the rim of Bonneville, their detection may be impeded by relief associated with the increased number of rocks >50 cm. Increasing rock size and abundance near the rim of Bonneville likely creates a clast-supported substrate (*20*) that may be more difficult to excavate during small impacts and leads to limited expression of near-rim hollows. The pristine appearance of Bonneville's ejecta deposits, however, makes it unlikely that near-rim hollows were formed and completely removed by erosion.

Once formed, hollows are rapidly modified to their present form. Their excavation during an impact is accompanied by emplacement of a surrounding ejecta deposit with widely varying grain size and fractured rocks (*19*). Surface roughness across these landforms would be in disequilibrium with the eolian regime (*15*), leading to deflation of ejected fines (fragments <2 mm in diameter), exposing fractured rocks, and creating a population of perched coarser fragments. At the same time, hollow interiors would be filled as transported fines are trapped within the depression. Trenching with Spirit's wheels in Laguna hollow near the edge of the Bonneville ejecta exposed unaltered basaltic fines (*16*, *22*) capped by a thin layer of brighter, finer, globally pervasive dust. The absence of dust interbeds or any chemical signature of dust in sediment filling the hollows, coupled with their uniformly filled appearance, implies rapid modification to their current more stable form.

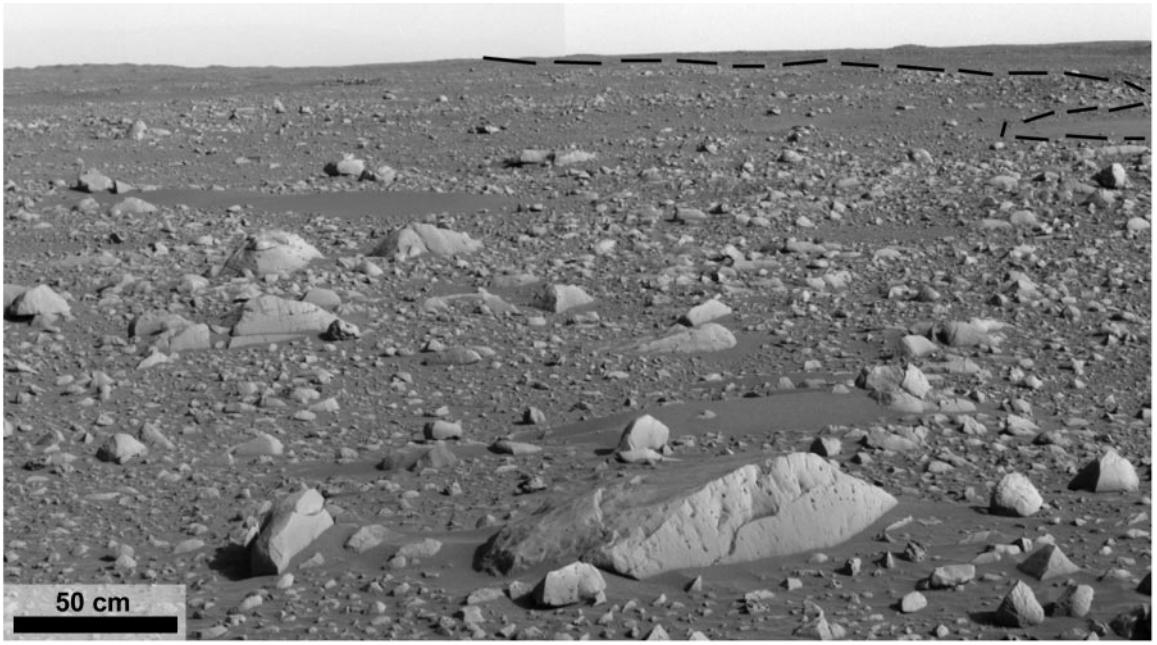

Fig. 2. Distal margin of Bonneville's ejecta deposit (black dashed line) from "Middle Ground" hollow. Mosaic of Pancam images 2P131526662FFL1155P2437 and 2P131526768FFL1155P2437 with the 430-nm blue filter.

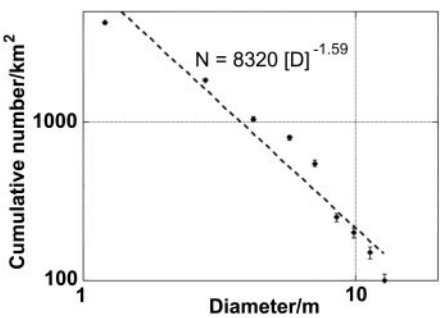

Fig. 3. Hollow size-frequency distribution along the traverse to Bonneville crater. Hollows are plotted in square root of 2 bins for the size range 20 m down to 1 m and reported as the number per km^2. Includes 85 hollows >0.02 km^2.

Surficial deposits created by impact and eolian processes are recognized in Gusev crater. Impact craters and associated ejecta deposits dominate the landscape and account for disruption of the upper ~10 m of the volcanic subsurface. The predominant role played by cratering processes in shaping the surface landforms is underscored by the impact origin of the hollows.

The shape, size, and clearly defined distribution of ejecta blocks >20 cm around Bonneville is generally consistent with observations around pristine terrestrial craters (*20*, *26*). Minor differences between observed rock populations and that expected from a single impact event are likely the result of comminution during multiple impacts that mix dark gray and lighter toned (presumably coated and/or more weathered) rocks (*10*, *16*, *27*). Although the hollows are modified, their diameters and associated implied depths (*21*) suggest meters or less of infilling. Some local redistribution of rocks <10 cm and/or winnowing of fines to form pavements [figure 4 in (*28*)] may account for lesser along-traverse variation in these size fragments but is also consistent with only meters of gradation at most. Hence, relief on the plains appears to be created by rubble accumulated in the aftermath of multiple impact events, and morphology diagnostic of nonimpact processes is not preserved.

All of the surficial deposits are basaltic, and their uniform composition (*16*) argues for a local volcanic source. If the rocks at the landing site were delivered by large impacts outside of Gusev or alluvial transport out of the Ma'adim Vallis watershed [which exceeds 200,000 km^2 along the main channel alone (*7*)], they would sample a range of terrains and have variable chemistry (at least in trace elements), which is not seen. Moreover, the size, poor sorting, and rounding of the largest rocks makes their arrival as alluvium from Ma'adim Vallis unlikely. Estimated discharge (*29*) and derived flow velocity (*30*) for Ma'adim Vallis indicate that rocks >1 m could not have been transported tens of kilometers to the landing site by clear water or hyperconcentrated flows. Finally, it is unlikely that the numerous rocks larger than 1 to 2 m could be ejecta coming from outside of Gusev, because they would not survive ballistic sedimentation (*19*). While no obvious fissure or other volcanic edifice is visible on the floor of Gusev crater, plains to the northeast have been interpreted as volcanics (*31*) that may have extended into the landing region but were broken up during subsequent impacts.

Local eolian deposits are inactive in the current setting (*15*). Although past eolian activity must have accounted for drift migration, formation of numerous faceted rocks, and infilling of hollows, and is another means of creating light-toned rocks (*15*), the local distribution of eolian deposits indicates that eolian processes are subordinate to impact processes in shaping the surface.

While conclusive evidence for ancient water-lain deposits in Gusev remains elusive, the volcanic materials and subsequent action of impact and eolian processes may mask their signature across terrains traversed during the nominal mission. Nevertheless, the preservation of the landscape is testament to the minimal gradation occurring since Hesperian times in Gusev that may be roughly comparable to post-Hesperian gradation affecting the Mars Pathfinder landing site (*32*).

References and Notes

1. M. P. Golombek *et al.*, *J. Geophys. Res.* **108**, 8072 (2003).
2. J. A. Grant *et al.*, *Planet. Space Sci.* **52**, 11 (2004).
3. N. A. Cabrol, E. A. Grin, G. Dawidowicz, *Icarus* **123**, 269 (1996).
4. N. A. Cabrol, E. A. Grin, R. Landheim, *Icarus* **132**, 362 (1998).
5. N. A. Cabrol, E. A. Grin, R. Landheim, R. O. Kuzmin, R. Greeley, *Icarus* **133**, (1998).
6. R. O. Kuzmin, R. Greeley, R. Landheim, N. A. Cabrol, J. Farmer, *U.S. Geol. Surv.*, Misc. Geol. Invest. Map **I-2666** (2000).
7. R. P. Irwin, T. A. Maxwell, A. D. Howard, R. A. Craddock, D. W. Leverington, *Science* **296**, 2209 (2002).
8. J. W. Rice Jr. *et al.*, *Lunar Planet. Sci.* [CD-ROM], abstract 2091 (2003).
9. Names have been assigned to areographic features by the Mars Exploration Rover (MER) team for planning and operations purposes. The names are not formally recognized by the International Astronomical Union.
10. J. F. Bell III *et al.*, *Science* **305**, 800 (2004).
11. M. P. Golombek, D. Rapp, *J. Geophys. Res.* **102**, 4117 (1997).
12. M. P. Golombek *et al.*, *J. Geophys. Res.* **108**, 8086 (2003).
13. M. R. Leeder, *Sedimentology*, George Allen and Unwin Ltd. (London, 1982).

14. R. L. Folk, *Petrology of Sedimentary Rocks*, Hemphill Publishing (Austin, TX, 1980).
15. R. Greeley *et al*., *Science* **305**, 810 (2004).
16. H. Y. McSween *et al*., *Science* **305**, 842 (2004).
17. M. P. Golombek *et al*., *Lunar Planet. Sci.* [CD-ROM], abstract 2185 (2004).
18. K. E. Herkenhoff *et al*., *Science* **305**, 824 (2004).
19. H. J. Melosh, *Impact Cratering*, Oxford Univ. Press (New York, 1989).
20. J. A. Grant, P. H. Shultz, *J. Geophys. Res.* **98**, 11025 (1993).
21. M. Hurst, M. P. Golombek, R. Kirk, *Lunar Planet. Sci.* [CD-ROM], abstract 2068 (2004).
22. R. E. Arvidson *et al*., *Science* **305**, 821 (2004).
23. W. K. Hartmann, J. Anguita, M. A. de la Casa, D. C. Berman, E. V. Ryan, *Icarus* **149**, 37 (2001).
24. W. K. Hartmann *et al*., *Nature* **397**, 586 (1999).
25. F. Horz, M. J. Cintala, W. C. Rochelle, B. Kirk, *Science* **285**, 2105 (1999).
26. J. A. Grant, P. H. Schultz, *J. Geophys. Res.* **98**, 15033 (1993).
27. P. R. Christensen *et al*., *Science* **305**, 837 (2004).
28. S. W. Squyres *et al*., *Science* **305**, 794 (2004).
29. R. P. Irwin, A. D. Howard, T. A. Maxwell, *Lunar Planet. Sci.* [CD-ROM], abstract 1852 (2004).
30. G. Komatsu, V. R. Baker, *J. Geophys. Res.* **102**, 4151 (1997).
31. K. A. Milam *et al*., *J. Geophys. Res.* **108**, 8078 (2003).
32. M. P. Golombek, N. T. Bridges, *J. Geophys. Res.* **105**, 1841 (2000).
33. Research was supported by NASA through the Mars Exploration Rover Project. Our sincere thanks go to the Mars Exploration Rover management, staff, and engineering teams for their outstanding support and operation of Spirit.

Plates Referenced in Article

www.sciencemag.org/cgi/content/full/305/5685/807/DC1

Plates 1, 3, 5, and 9

3 May 2004; accepted 28 June 2004

REPORT

Wind-Related Processes Detected by the Spirit Rover at Gusev Crater, Mars

R. Greeley,[1] S. W. Squyres,[2] R. E. Arvidson,[3] P. Bartlett,[4] J. F. Bell III,[2] D. Blaney,[5] N. A. Cabrol,[6] J. Farmer,[1] B. Farrand,[7] M. P. Golombek,[5] S. P. Gorevan,[4] J. A. Grant,[8] A. F. C. Haldemann,[5] K. E. Herkenhoff,[9] J. Johnson,[9] G. Landis,[5] M. B. Madsen,[10] S. M. McLennan,[11] J. Moersch,[12] J. W. Rice Jr.,[1] L. Richter,[13] S. Ruff,[1] R. J. Sullivan,[2] S. D. Thompson,[1] A. Wang,[3] C. M. Weitz,[14] P. Whelley,[1] Athena Science Team

Wind-abraded rocks, ripples, drifts, and other deposits of windblown sediments are seen at the Columbia Memorial Station where the Spirit rover landed. Orientations of these features suggest formative winds from the north-northwest, consistent with predictions from atmospheric models of afternoon winds in Gusev Crater. Cuttings from the rover Rock Abrasion Tool are asymmetrically distributed toward the south-southeast, suggesting active winds from the north-northwest at the time (midday) of the abrasion operations. Characteristics of some rocks, such as a two-toned appearance, suggest that they were possibly buried and exhumed on the order of 5 to 60 centimeters by wind deflation, depending on location.

In the current environment of Mars, wind appears to be the most frequent agent of surface modification, resulting in albedo patterns that change on time scales as short as a few weeks (*1*). Abundant dune forms, mantles of windblown deposits, and wind-eroded features are seen from orbit in many parts of Mars, including the three previous sites where successful landings have occurred. Understanding the processes that form aeolian (wind-related) features provides insight into the evolution of the martian surface, including rates of erosion and deposition. The Mars Exploration Rover (MER) Spirit landed near the middle of Gusev Crater (*2*–*5*) in a relatively low-albedo zone (*6*) considered to be a track left by the passage of dust devils that removed bright dust to expose a relatively darker substrate (Fig. 1A). Comparison of orbital images taken of the same area from July 2003 to January 2004 show changes in the tracks, indicating that dust devils were recently active.

Here, we describe initial analyses of aeolian features during the first ~90 sols (*7*) of operation. Wind-related features include sediments (some of which are organized into bedforms such as ripples), wind-abraded features on rocks, eroded zones around rock edges, and features generated by the rover during operations that suggest active winds.

The surface at Columbia Memorial Station consists of rocks, regolith, dark granules, and fine-grained material, including dust (*8*, *9*). Patches of red regolith range in size from 0.5 m across to as large as 15 m across. Bonneville (*10*) crater and many of the small depressions, called hollows, are partly filled with regolith deposits. Light-toned material was inferred to be dust, the upper surfaces of some rocks, the rover solar panels, and the Panoramic Camera (Pancam) calibration target (*11*). Although dust grains are too small to be resolved by the Microscopic Imager (MI) (*12*), previous estimates suggest that martian dust is a few micrometers in diameter (*13*, *14*).

An MI image of a regolith patch shows a bimodal size distribution of particles (Fig. 1B) that includes coarse (1 to 3 mm) grains and finer grains smaller than a few hundred micrometers in diameter. Although some coarse grains are subangular, most are rounded, suggesting erosion during transport. We propose that the dark coarse particles are lithic fragments on the basis of their basaltic composition (*16*, *17*) and appearance in the MI images (*18*).

Aprons of granular debris occur as isolated patches on the regolith and around some rocks. For example, the rock Adirondack (*2*) has an encircling debris apron that extends 5 to 20 cm from the edge of the rock. The aprons consist of coarse grains that have spectral properties similar to those of Adirondack and the other basaltic rocks in the area (*11*, *19*). Therefore, some of the more angular coarse-grained material is probably derived

[1]Department of Geological Sciences, Arizona State University, Box 871404, Tempe, AZ 85287–1404, USA. [2]Department of Astronomy, Cornell University, 428 Space Sciences Building, Ithaca, NY 15853–1301, USA. [3]Department of Earth and Planetary Sciences, Washington University, One Brookings Drive, St. Louis, MO 63031–4899, USA. [4]Honeybee Robotics, 204 Elizabeth Street, New York, NY 10012, USA. [5]Jet Propulsion Laboratory, 4800 Oak Grove Drive, Pasadena, CA 91109–8099, USA. [6]Ames Research Center, Moffett Field, CA 94035–1000, USA. [7]Space Science Institute, University of Colorado, Boulder, CO 80301, USA. [8]Center for Earth and Planetary Studies, National Air and Space Museum, Smithsonian Institution, Washington, DC 20560–0315, USA. [9]U.S. Geological Survey, 2255 North Gemini Drive, Flagstaff, AZ 86001–1698, USA.[10]Niels Bohr Institute for Astronomy, Physics, and Geophysics, Center for Planetary Science and Ørsted Laboratory, University of Copenhagen, Universitetsparken 5, DK-2100 Copenhagen, Denmark. [11]Department of Geosciences, State University of New York at Stony Brook, Stony Brook, NY 11794–2100, USA. [12]Department of Earth and Planetary Sciences, University of Tennessee, 1412 Circle Drive, Room 306, Knoxville, TN 37996, USA. [13]Deutches Zentrum für Luft-und Raumfart (German Aerospace Center)–Institute of Space Simulation, Linder Hoene, D-51170 Cologne, Germany. [14]National Aeronautics and Space Administration (NASA) Headquarters, Washington, DC 20546–0001, USA.

*To whom correspondence should be addressed. E-mail: Greeley@asu.edu